Effect of Densification on the Random Field Model Parameters of Liquefiable Soil and their Use in Estimating Spatially-Distributed Liquefaction-Induced Settlement

Armin W. Stuedlein, *Professor, Oregon State University, Corvallis, OR, U.S.A.; email: Armin.Stuedlein@oregonstate.edu*
Taeho Bong, *Research Fellow, Gyeonggi Research Institute, Suwon, Korea; email: bth21c@gri.re.kr*
Jack Montgomery, *Assistant Professor, Auburn University, Auburn, AL, U.S.A.; email: jmontgomery@auburn.edu*
Jianye Ching, *Professor, National Taiwan University, Taipei, Taiwan; email: jyching@gmail.com*
Kok-Kwang Phoon, *Professor, National University of Singapore, Singapore; email: kkphoon@nus.edu.sg*

ABSTRACT: *Densification-type ground improvement has gained wide acceptance as an effective technique to improve the static and cyclic strength and seismic performance of liquefiable soils. However, there has been little attempt to quantify the degree of change in certain measures of soil spatial variability following densification. This study uses the random field model (RFM) framework to quantify changes in the trend, inherent variability, and the autocorrelation of soil following various densification-based ground improvement methods using case history data. Ground improvement technologies investigated include driven displacement piles, vibro-replacement (i.e., stone columns), and deep dynamic compaction. Vertical RFM parameters are shown to change significantly following densification, with reductions in the coefficient of inherent variability, and increases in the scale of fluctuation, the latter of which appears related to the initial relative density. One case history is used to illustrate the utility of the RFM framework to link spatial variability of the post-shaking settlements to the results of a geostatistical model of the subsurface, including the three-dimensional distribution of CPT measurements and fines content. It is shown that the spatial distribution of differential surface settlements is correlated to those spatially-varying subsurface characteristics that are known to lead to larger liquefaction-induced settlement.*

KEYWORDS: densification, liquefaction, spatial variability, auto-correlation, random field model

SITE LOCATION: **Geo-Database**

INTRODUCTION

The consequences of earthquake-induced liquefaction have been recognized as a significant hazard to civil infrastructure since the mid-1960s following the 1964 Niigata and Good Friday (Great Alaskan) earthquakes. Liquefaction arises from the tendency of loose, saturated, clean to silty sands to contract under the transient shearing applied to these soils by vertically-propagating horizontal shear waves, which results in elevated excess pore pressures and the potential for large reductions in soil strength. Specialty contractors have since developed new, and adapted existing, methods to improve the strength and stiffness of liquefiable soils providing support to civil infrastructure, such as deep foundations, embankments, and other structures. Ground improvement methods generally fall within three broad categories including densification, reinforcement, and drainage (Stuedlein et al. 2016). Densification methods include vibro-compaction, vibro-replacement (i.e., stone columns), sand compaction piles, and drilled and driven displacement piles and are used to reduce the void space within soils by rearranging the soil particles into a denser state to increase the relative density and corresponding cyclic resistance.

Numerous studies have been conducted to quantify the increase in density due to densification-based ground improvements, the results of which commonly include a comparison of the pre- and post-treatment standard penetration test (SPT) penetration

Submitted: 20 October 2020; Published: 25 October 2021
Reference: Stuedlein A.W., Bong T., Montgomery J., Ching J., and Phoon K.K. (2021). Effect of Densification on the Random Field Model Parameters of Liquefiable Soil and their Use in Estimating Spatially-Distributed Liquefaction-Induced Settlement. International Journal of Geoengineering Case Histories, Volume 6, Issue 4, pp. 1-16, doi: 10.4417/IJGCH-06-04-01

resistance N or cone penetration test (CPT) corrected cone tip resistance, q_t (e.g., Plantema and Nolet 1957; Rollins et al. 2012; Stuedlein et al. 2016; Stuedlein and Allen 2018). Most studies have demonstrated a significant increase in measures of penetration resistance following densification-type ground improvement, and the magnitude of densification varies depending on the soil type, time since installation of the improvements, and the type of improvement installed. Although these studies have presented quantification of the increase in q_t, their statistical properties and the associated auto-correlation (i.e., spatial variability) also change. However, there has been little attempt to quantify the magnitude in the change of the autocorrelation or variability of soils after densification, or to connect the changes in the spatially-variable conditions to actual performance following a strong ground motion event. This observation presents a significant barrier to improving the understanding of the consequences of liquefaction and how they may be controlled by the specific geomorphological signatures of a given deposit. For example, the spatial variability of soil stratigraphy (e.g., azimuthally-dependent strata thickness) and inherent variability within a given stratum are consistently identified as being responsible for the distribution of damage observed following earthquakes (e.g., Cubrinovski et al. 2011) and presents a source of error in the accuracy of available procedures (e.g., Bong and Stuedlein 2018).

This paper uses case history data to seek an improvement in the understanding of the role of densification-based ground improvements to alter the spatially-variable characteristics of liquefiable soils and how the spatial distribution of the consequences of liquefaction might be predicted using random field model parameters describing the improved ground. First, four case studies that demonstrate the magnitude of densification of liquefaction-susceptible soil using CPTs conducted prior to and following improvement are presented. The ground improvement methods include conventional and drained, driven timber displacement piles, stone columns, and deep dynamic compaction. The random field model (RFM) framework was used to determine alterations in selected measures of spatial variability following densification such as the change in the trend, inherent variability, and the scale of fluctuation (a measure of autocorrelation length). Then, one of the case study sites where controlled blasting was conducted is further explored to determine if the spatially-variable post-shaking settlements can be linked to measures of the spatially-variable soil deposit that existed prior to, and exist following, densification. This study uses case history data to demonstrate that the consequences of liquefaction and their spatial distribution can indeed be predicted using random field theory and that investigations such as that presented herein may help to further understand the variability in liquefaction-induced displacements possible in future studies.

CASE HISTORIES CONSIDERED

Case History A: Driven Displacement Piles

Installation of driven displacement piles has been widely recognized to result in significant densification of loose granular soils (Meyerhof 1959; Robinsky and Morrison 1964; Broms 1966) and is commonly used as a ground improvement technique (Sy 2018). Driven timber piles comprise the ground improvement type for Case History A, which includes Case A-1, where the performance of conventional and drained timber piles to densify liquefiable soils was conducted at a test site in Hollywood, SC, and Case A-2, which considers the application of conventional timber piles to densify liquefiable soils below a four-story structure situated in Mt. Pleasant, SC. The subsurface conditions for these two cases are similar: the liquefiable layers consisted of an upper deposit of clean, fine sand (ranging in thickness from 2 to 6 m), transitioning to a lower deposit of sand and silty sand with thicknesses of 4 to 6 m. The groundwater tables at the two sites were generally observed at 1 to 2 m depth below the ground surface.

Case A-1 considers five treatment zones, including Zones 1 and 2 using timber piles fitted with pre-fabricated drains used in an attempt to improve the densification possible in silty sands, and Zones 3, 4, and 5B, which considered conventional timber displacement piles. The piles were installed in a square configuration and the main experimental variable considered in both cases was the spacing of the piles, which included spacings of 5D (Zones 1 and 3), 4D (Zone 5B), and 3D (Zones 2 and 4), where D is the pile head diameter. The head and toe diameters of the piles driven as part of Case A-1 were 310 and 210 mm, respectively, and their length was 12 m. General and specific information for Case A-1 as relates to the subsurface characterization, densification program, controlled blasting experiments, and geostatistical modeling of the subsurface has been systematically reported by Stuedlein et al. (2016), Stuedlein and Gianella (2016), Gianella and Stuedlein (2017), and Bong and Stuedlein (2017; 2018); the interested reader is referred to these studies.

Described in Stuedlein et al. (2016), the pile locations were pre-drilled to depth of approximately 2 to 3 m to reduce the driving resistance within the near-surface fill soils, which contained construction debris (e.g., wood, brick, and other residential construction materials). The area replacement ratio, a_r, driving sequence, and depths of embedment varied for each treatment zone and within a given treatment zone as listed in Table 1. The site was relatively level (within 50 mm over 30

m), and the strata thickness and its azimuthal extent was consistent across the site. The soils investigated in this study are limited to the liquefiable layers (Figure 1), which generally range in depth from 2.5 to 11 m. The depth of soil investigated using random field theory (RFT) ranges from 2.5 m to the average depth of treatment of the inner piles comprising each five-by-five pile group (Table 1) and correspond to conditions observed 8 months after pile installation (Stuedlein et al. 2016) except where noted otherwise below.

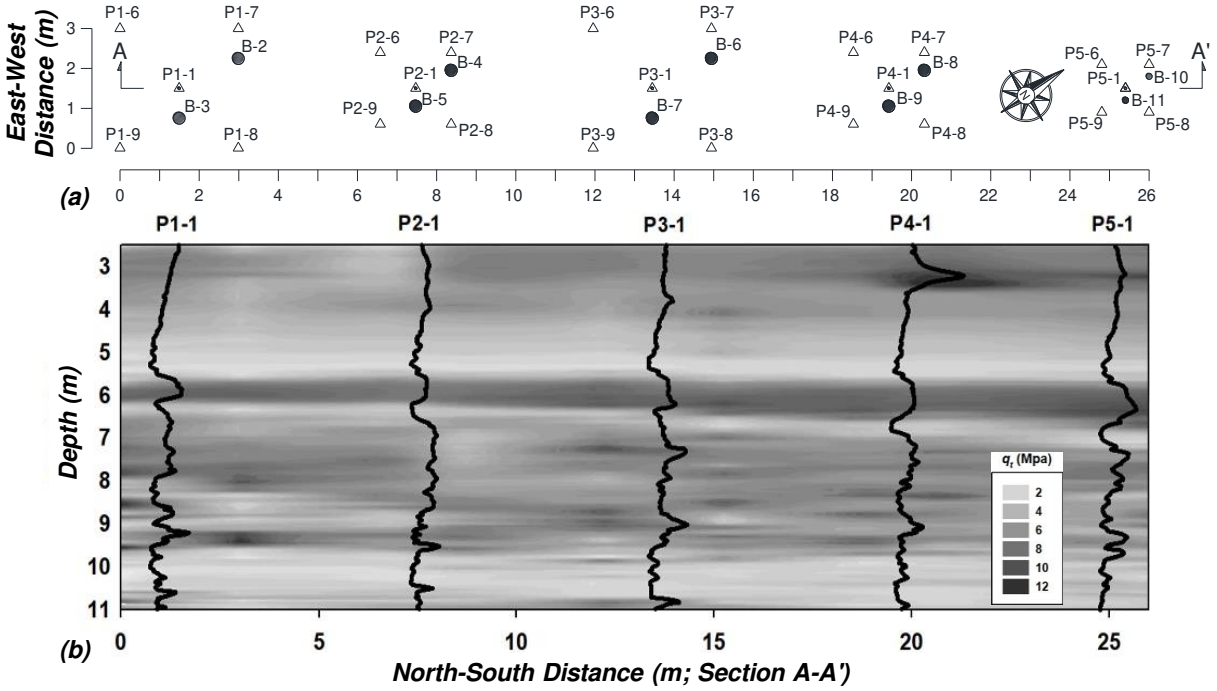


Figure 1. Site and subsurface conditions at the Hollywood, SC test site (Case A-1) including: (a) exploration plan for Zones 1 – 5, and (b) pre-treatment CPT cone tip resistance measured within the liquefiable layers along Section A-A' and corresponding spatial variation inferred from geostatistical analyses reported by Bong and Stuedlein (2017; 2018).

The timber piles assessed in Case A-2 and reported by Stuedlein and Allen (2018) consisted of two treatment zones: these were groups of piles arranged in a triangular spacing of 4.9*D* and 7.3*D*. The pile lengths were 6 m and were installed at locations that were pre-drilled to a depth of 0.6 m. The contractor used a follower to drive the pile heads 0.3 m below the adjacent ground surface elevation. The pile head and toe diameters were 250 and 200 to 225 mm, respectively. CPTs were performed prior to and one and two days following treatment in each of the two treated areas to depths of 6.4 m. It is important to recognize that the taper of timber piles (approximately 8 mm/m) results in a depth-dependent area replacement ratio, defined as the ratio of the area comprising the treatment (e.g., the piles) to the total area improved. Thus, the mean a_r varied for each of the timber pile-based densification cases assessed herein. Furthermore, lateral stresses relaxed (i.e., decreased) in the months following treatment, which is attributed to possible exposure to high shearing stresses and strain rates at the pile toe during installation (Stuedlein et al. 2016; Stuedlein and Allen 2018), and this effect may be observed in penetration test results. Thus, the effect of time on the RFM parameters should be considered in their development, as described herein. The duration between the pre- and post-treatment CPTs for Case A-2 was two days.

Case History B: Vibro-Stone Columns

Improvements to an existing wastewater treatment plant located in Tacoma, WA included the use of vibro-stone column ground improvement placed below storage and treatment tanks to meet seismic deformation performance criteria. The subsurface profile included recent, interbedded sandy silt to silty sand, sand, and clayey silt to silty clay deposits characteristic of Puyallup alluvium (Stuedlein 2010). Explorations revealed the groundwater table was located 3 m below the ground surface. Vibro-stone columns (SC) with a diameter of 1.07 m were installed within a square arrangement on 2.44 m centers and distributed over 1,700 m^2 to densify liquefiable soils and reinforce soft, plastic soils. The a_r corresponding to this case history was 15% (Table 1). The stone columns were installed prior to the excavation of soils that existed above the tank footprints, and varied in finished depth-of-treatment from 3.7 to 6.7 m. Four pairs of pre- and post-treatment CPTs were

performed to depths of 12 m, extending through the upper excavation zone and below the lower untreated elevations to assess liquefaction mitigation requirements. The duration between the pre- and post-treatment CPTs for Case B was one month.

Table 1. Summary of CPTs conducted to evaluate the performance of densification-type ground improvements.

Method	Soil type	Test area	Depth range (m)	Average area replacement ratio, a_r (%)	Mean q_t (MPa)		Change in q_t (%)
					Pre-treatment	Post-treatment	
Drained timber pile (Case A-1)	Sand, Silty sand	Zone 1	2.5 ~ 12.1	2.05	4.60	6.37	38.2
		Zone 2	2.5 ~ 9.3	6.23	5.34	14.35	169.0
		Zone 3	2.5 ~ 11.7	2.08	5.29	6.49	22.8
		Zone 4	2.5 ~ 11.1	5.89	5.59	9.63	72.4
		Zone 5B	2.5 ~ 10.6	3.37	6.15	11.40	85.4
Timber pile (Case A-2)	Sand	CPT T1	0.5 ~ 6.4	3.2	5.25	9.62	83.2
		CPT T2	0.5 ~ 6.4	1.4	5.49	7.46	35.7
Stone Column (Case B)	Sandy silt, Silty sand, Sand, Clayey silt	CPT S1	2.1 ~ 8.7	15.0	4.37	10.82	147.6
		CPT S2	2.1 ~ 8.5	15.0	3.86	10.50	172.1
		CPT S3	2.1 ~ 8.4	15.0	5.13	10.21	98.8
		CPT S4	2.3 ~ 9.0	15.0	4.44	7.37	65.9
Deep Dynamic Compaction (Case C)	Sand, Silty Sand	CPT-1A	0.5 ~ 6.0	-	10.00	17.77	77.7
		CPT-1B	0.5 ~ 6.0	-	21.93	23.01	4.9
		CPT-2A	0.5 ~ 6.0	-	15.65	21.44	37.0
		CPT-2B	0.5 ~ 6.0	-	21.09	23.09	9.5
		CPT-3A	0.5 ~ 6.0	-	18.13	25.33	39.7
		CPT-3B	0.5 ~ 6.0	-	18.36	20.68	12.6
		CPT-4A	0.5 ~ 6.0	-	12.91	21.57	67.2
		CPT-4B	0.5 ~ 6.0	-	23.40	21.99	-6.0

Case History C: Deep Dynamic Compaction

Deep dynamic compaction (DDC) was used to improve the strength and stiffness of soils supporting wind turbine foundations in the town of Bourne, MA. These soils generally consisted of non-plastic, granular, medium dense, fine to medium sand and silty sand transitioning to medium to coarse sand in the upper 15 m, and grading to sand and gravel to 32 m depth. The depth of the groundwater table was approximately 20 m. Due to the seismic setting and depth of the groundwater table, liquefaction did not pose a significant hazard for this case history; nonetheless, the soils are similar to those possibly subject to liquefaction in other geological settings and are included for the analyses conducted herein. The shallow mat foundations were shaped in an octagon and ranged in width from 16.9 to 17.8 m. Requirements for bearing pressure performance led to the use of DDC to improve the ground to depths of up to 6 m.

The specialty contractor used one high energy pass with a 1.5 m diameter, 10 ton tamping weight falling 15 m distributed on a 2.7 m grid. Each high energy tamping grid point was proposed to be tamped a minimum of 10 times within and extending 4 m beyond the octagonal mat foundation footprint to result in a total of 281 kJ of treatment. Impact craters were filled and graded using compacted structural fill following each day of high-energy tamping. The densification was assessed using eight pairs of pre- and post-treatment CPTs conducted to 6 m depth (Table 1). The duration between the pre- and post-treatment CPTs for Case B was seven days. Comparison of the pre- and post-improvement CPTs in Table 1 indicates that initially denser soils generally exhibited smaller improvement in q_t, which was likely a result of dilation-induced shearing (heave) resulting from the high energy pass that was not fully rectified during the compaction of the placed structural fill. This aspect is discussed in greater detail below.

RANDOM FIELD THEORY (RFT), MODEL PARAMETERS, AND AUTOCORRELATION MODELS

Random field theory (RFT) provides a suitable and succinct framework for the characterization of the spatial variability of soils (Vanmarcke 1983), which is known to frequently control the geotechnical response of geostructures owing to the concentration of strains within locally softer and weaker portions of the soil deposit (Fenton and Vanmarcke 1998; Griffiths and Fenton 2001; Montgomery and Boulanger 2016; Bong and Stuedlein 2018). The inherent variability of a soil property,

for example CPT q_t, can be characterized using random field model (RFM) parameters and include the depth-dependent trend function, the coefficient of inherent variability, COV_w, and the scale of fluctuation, δ, which is a measure of the autocorrelation distance of the property (Vanmarcke 1977; 1983). The depth-dependent trend function is readily determined using ordinary least squares (OLS) regression (as shown in Figure 2) and was computed, along with the mean q_t, over the depth interval shown in Table 1. The COV_w is equal to the ratio of the standard deviation of the detrended residuals (e.g., difference between q_t and its trended magnitude) normalized by the trended or mean magnitude, and represents the fluctuating component of the measured soil property. As recently summarized by Cami et al. (2020), several methods exist to estimate the scale of fluctuation, δ, such as the: (1) expeditive method (Vanmarcke 1977); (2) variance reduction function (Vanmarcke 1977); (3) intersection of the sample autocorrelation function (ACF) with the Bartlett's limit (Jaksa 1995); and (4) fitting of residuals to an autocorrelation model (Vanmarcke 1977). Among these possibilities, the autocorrelation model fitting (AMF) method provides an expedient and methodical approach and is performed by fitting a theoretical autocorrelation model to the experimental or sample correlation function using OLS or another approach. The sample autocorrelation function at a lag or separation distance τ between two observations may be computed using:

$$\rho(\tau) = \frac{\sum_{i=1}^{n(\tau)}(X_i-\bar{X})(X_{i+\tau}-\bar{X})}{\sum_{i=1}^{N}(X_i-\bar{X})^2} \quad (1)$$

where X_i is the value of property X at location i, $\bar{X}$ is the mean of the property X, N is the number of measurements, and $n(\tau)$ denotes the number of data pairs that are separated by the lag distance τ. The expressions for the theoretical autocorrelation models considered herein are summarized in Table 2, and consist of the single exponential (SNX), cosine exponential (CSX), second-order Markov (SMK), and squared exponential (SQX) models, due to their frequency of use in geotechnical applications (Uzielli et al., 2005; Stuedlein et al. 2012). In this approach, δ is computed directly from the fitted autocorrelation model parameter associated with each model (Table 2). The procedure used to determine δ through fitting to the models in Table 2 is presented in Figure 2. In summary, the RFM parameters necessary to fully describe the random field characteristics of a given soil deposit include the trend function of the measurement, its COV_w, and δ.

Table 2. Autocorrelation models and corresponding scale of fluctuation; τ = lag distance.

Autocorrelation Model	Equation	Scale of Fluctuation, δ
SNX	$\rho(\tau) = \exp(-\lambda\|\tau\|)$	$2/\lambda$
CSX	$\rho(\tau) = \exp(-b\|\tau\|)\cos(b\tau)$	$1/b$
SMK	$\rho(\tau) = (1 + d\|\tau\|)\exp(-d\|\tau\|)$	$4/d$
SQX	$\rho(\tau) = \exp[-(a\tau)^2]$	$\sqrt{\pi}/a$

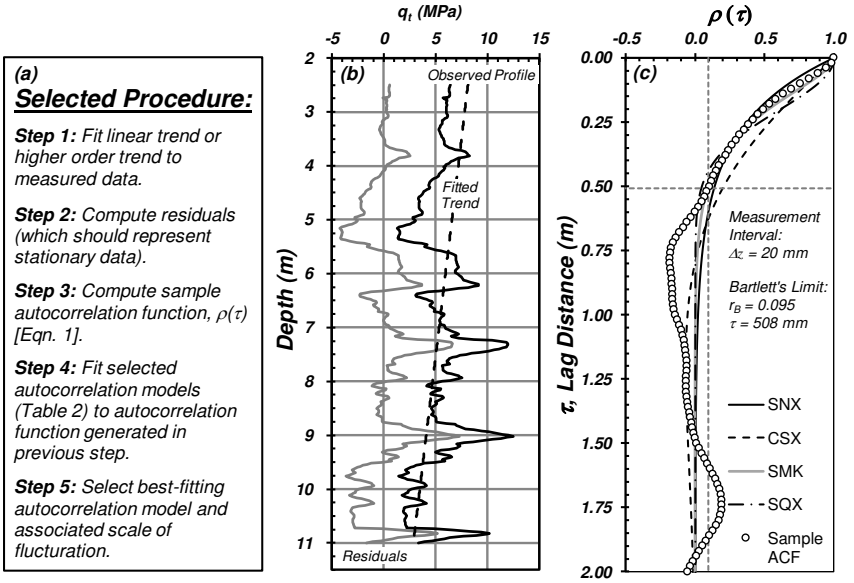


Figure 2. Demonstration of the procedure used to determine the scale of fluctuation for CPT P3-1 (Case A-1): (a) procedure steps; (b) observed and detrended q_t; and (c) corresponding sample ACF and fitted autocorrelation models.

Comparison of Pre- and Post-Improvement CPT Cone Tip Resistances

Performance-based ground improvement contracts are typically centered on requirements to achieve a particular performance goal, which lends flexibility to the contractor when selecting the type of ground improvement and such design variables as the area replacement ratio. Performance goals may consist of one or more of the following metrics: (1) achieving a minimum factor of safety against liquefaction triggering, FS_L, (2) achieving a particular quantile (e.g., 90%) of a minimum FS_L, (3) limiting post-liquefaction settlements to a certain threshold magnitude (e.g., 5 cm), or other criteria. Regardless of the performance metric used to confirm that a particular level of ground improvement has been achieved, *in-situ* tests are generally the vehicle by which the metric is quantified. Thus, comparison of nearby *in-situ* test results corresponding to the pre- and post-improvement conditions provide an effective means by which to judge if a particular performance goal has been achieved (Slocombe et al. 2000; Stuedlein et al. 2016). Figure 3 presents examples of the comparison of the pre- and post-treatment q_t profiles from case histories A-1, A-2, B, and C. Review of Figure 3 indicates that significant densification was achieved for these cases, although variation in treatment was observed as a function of the spacing of treatments, fines content, and other factors (Table 1). In the assessments that follow, changes in the global mean, trend function, coefficient of inherent variability, and scale of fluctuation are evaluated and compared.

Effect of Densification on the Mean, Trend Function, and Fluctuating Component of Vertical Spatial Variability

Figure 4 compares the pre- and post-treatment average q_t; the standard deviation of detrended q_t ($q_{t\text{-}det}$), representing the residual q_t, defined as the difference between the measured and depth-dependent trend in q_t; and the corresponding coefficient of inherent variability in q_t, $COV_{w,v}(q_t)$. Figure 4a demonstrates that the mean q_t increased substantially for most cases, with an average increase in mean q_t equal to 78, 59, 121, and 30% for Cases A-1, A-2, B, and C, respectively. In one case, CPT-4B (Case C) decreased slightly; this particular exploration exhibited the largest pre-treatment cone tip resistance of the assembled cases (Table 1), and the soils may have dilated on average due to DDC. Estimation of such RFM parameters as δ_v and $COV_{w,v}$ requires careful selection of a trend function. Herein, the trend function was selected by considering the change in the sample ACF following progressive increase in the order of trend removed (e.g., linear, 2nd order polynomial, etc.) as suggested by Jaksa (1995) and the stress history of the soil. For example, normally-consolidated clays should exhibit relatively linear increases in measures of soil strength or penetration resistance with depth, whereas aged or overconsolidated soil profiles may exhibit highly-nonlinear trends (Jaksa et al. 1997; Stuedlein et al. 2012).

For many of the cases evaluated, the type of trend function in q_t changed following densification. Initially, most of the pre-treatment q_t profiles were suitably characterized using a linear trend; following densification, most of the profiles were best characterized using a quadratic trend, which is consistent with a tendency for soils to exhibit marked overconsolidation as a result of densification (Mayne and Kulhawy 1982; Massarsch 2020). The main distinctions between soils that are geologically overconsolidated and densified is that in the latter case, the duration of the maximum past pressure is ephemeral and more appropriately considered using the concept of mean effective stress. Naturally, the soil type at the site (generally sands and silty sands for densification-based improvements) and area replacement ratio control the increase in penetration resistance, whereas the type of densification (e.g., vibro-compaction vs. top-down DDC) will contribute to the dependency of that increase with depth.

Figure 4b shows that the standard deviation in the detrended q_t increased following improvement, apart from some cases in the DDC case history. This stems from the presence of interbedded silty sands, sandy silts, and/or plastic silts and clays present in Cases A-1, A-2, and B, which can inhibit densification due to poor drainage (Rollins et al. 2006; Stuedlein et al. 2015; 2016). The standard deviation can be used as indicator of the role of such layered soils to inhibit densification. However, $COV_{w,v}(q_t)$ decreased by 14, 19, 14, and 22% for Cases A-1, A-2, B, and C, respectively, on average, which results from an offset of the increases in the standard deviation by the increases in the mean q_t. Thus, the initial inherent variability of mechanical soil properties decreases as a direct consequence of densification-based ground improvement, and the $COV_{w,v}$ serves to provide a more appropriate measure of the global response of the treated depths to densification.

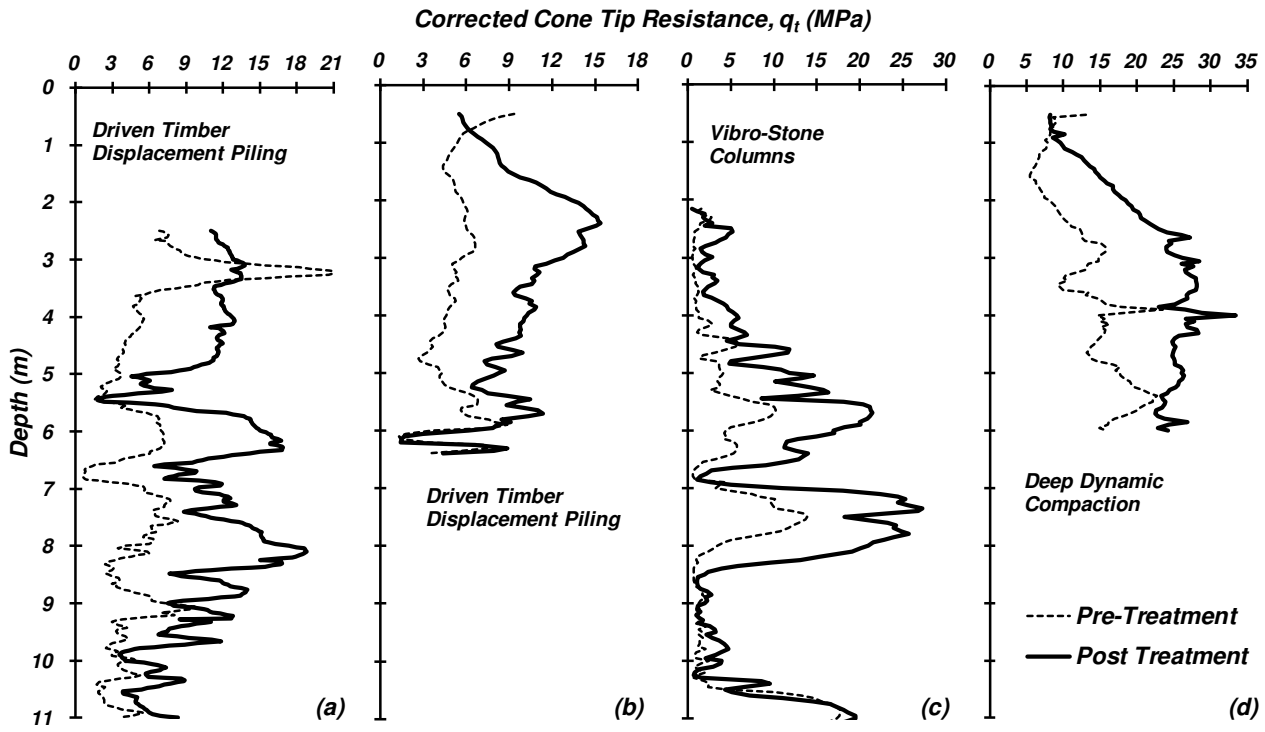


Figure 3. Comparison of representative pre- and post-installation corrected cone tip resistance profiles for (a) Case A-1 (Zone 4), (b) Case A-2 (CPT T1), (c) Case B (CPT S2), and (d) Case C (CPT-4A).

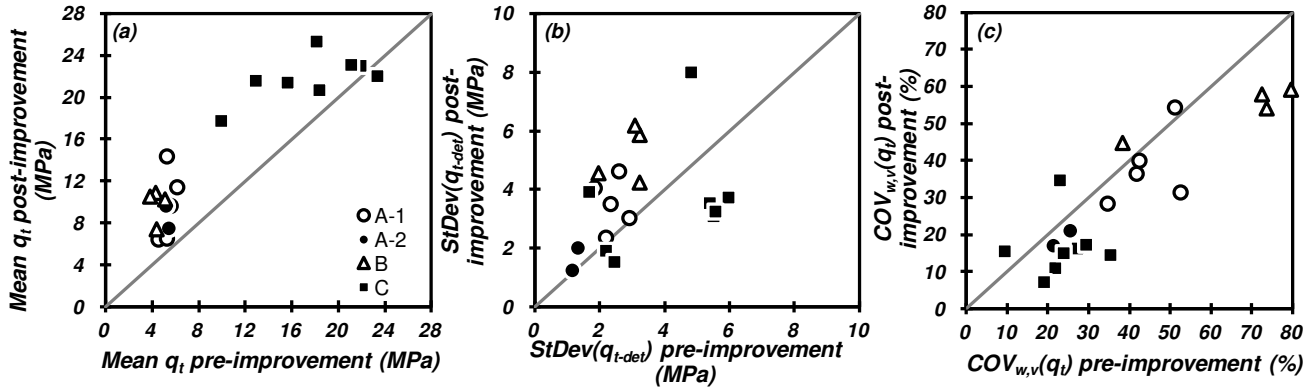


Figure 4. Comparison of pre- and post-installation: (a) mean q_t, (b) standard deviation in detrended q_t, $q_{t\text{-}det}$, and (c) coefficient of inherent variability, $COV_{w,v}(q_t)$.

Effect of Densification on the Vertical Scale of Fluctuation

Figure 5 presents the comparison of the pre- and post-treatment vertical scale of fluctuation, δ_v for q_t. In general, δ_v decreased by 2 to 43% (Fig 5a) for six CPTs, whereas it increased by 17 to 286% for 13 CPTs. An increase in δ_v indicates that the vertical homogeneity of the soil layer increased following densification, as soils exhibit a greater distance for which the measured penetration resistance is correlated with itself. Generally, densification resulted in an increase in the average δ_v for all cases (Fig. 5b). This is notable considering the markedly different densification techniques; however, the range in change of δ_v was large as shown in Fig. 5b. Slocombe et al. (2000) noted that CPT cone tip resistance appeared to increase with time since densification with vibro-stone columns (used in Case B), whereas Stuedlein et al. (2016) pointed to the relaxation of lateral stresses over time following densification with driven displacement piles. Thus, it is of interest to investigate whether the changes observed in typical RFM parameters, such as the scale of fluctuation, are likewise sensitive to time. Figure 5c

explores this question for Case A-1 through the comparison of the post-improvement δ_v computed from independent CPTs pushed 10 days following densification with driven displacement piles to that determined from q_t measurements performed 8 months after densification and reported by Stuedlein et al. (2016). Some treatment zones exhibited an increase in δ_v of up to 32% with time, whereas other treatment zones exhibited a decrease (up to 16%). Possible correlation between the change in δ_v with time and a_r was investigated and no significant effect was observed, pointing to other factors that may potentially contribute to a time-dependent variation in δ_v, or differences associated with the spatial variability of the soil itself.

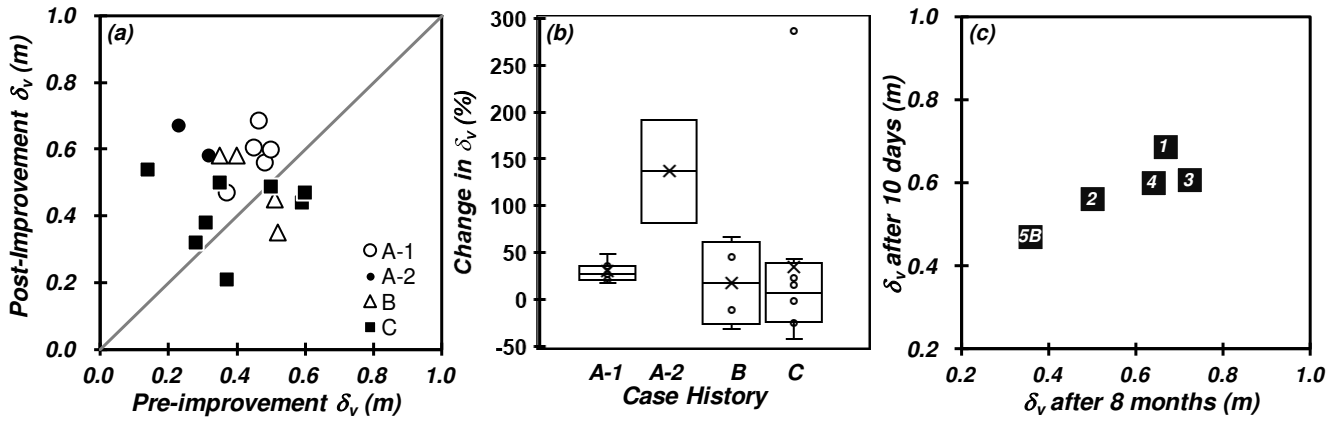


Figure 5. Evaluation of densification on the scale of fluctuation: (a) comparison of pre- and post-installation δ_v, (b) range in change of δ_v, and (c) effect of time on δ_v for Zones 1 through 5B for Case A-1 (see Table 1).

The increase in spatial homogeneity following densification appears to be related to the magnitude of initial spatial autocorrelation, as shown in Fig. 6a. The increase in δ_v following improvement is largest for those soil deposits where the initial scale of fluctuation is smallest, and the increase is smallest for those loose deposits where the initial δ_v is largest, regardless of the ground improvement technique implemented. Thus, soil deposits with low spatial homogeneity (small δ_v) will experience the greatest increase in autocorrelation length following densification. In addition, Fig. 6b shows that the change in mean q_t appears dependent on the pre-improvement mean q_t; in other words, the magnitude of densification that is possible appears larger for initially looser soils, consistent with anecdotal observations by ground improvement contractors and fundamental observations on the drained response of granular soils to shear (e.g., Youd 1972). No correlation between the change in δ_v and initial mean q_t was observed, indicating that the initial density of the deposit with its characteristic spatial autocorrelation does not contribute to the final, post-treatment autocorrelation length. Future research to ascertain whether a specific densification technique may be associated with characteristic RFM parameter magnitudes and/or area replacement ratios appears warranted.

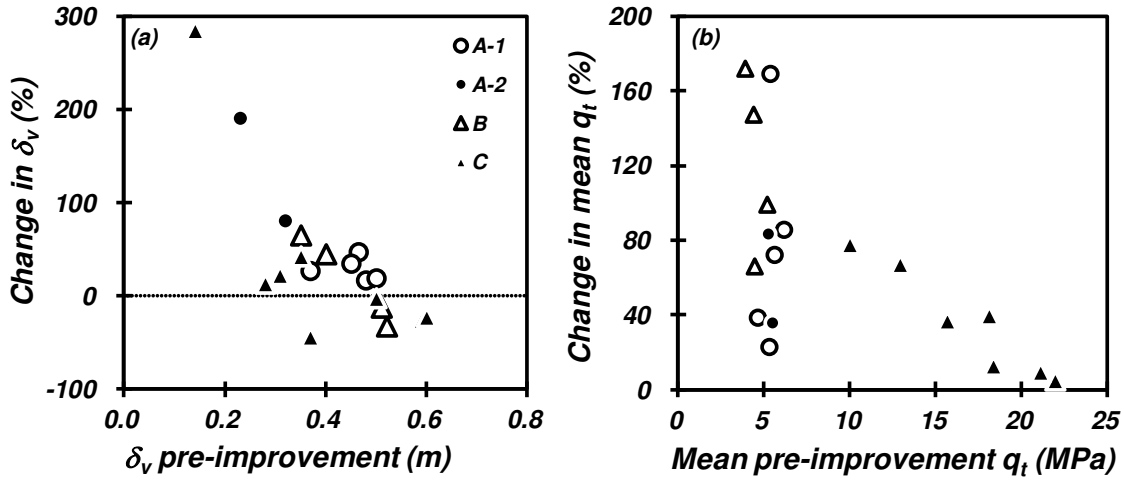


Figure 6. Post-treatment changes in: (a) δ_v as a function of the initial autocorrelation, and (b) mean q_t as a function of initial mean q_t.

It is of interest to the profession to understand whether increased site characterization, particularly towards quantification of the spatial variability in a robust manner such as that possible with random field theory (RFT), can serve to improve the understanding of the response of a soil deposit to strong ground motions associated with earthquakes. Case A-1 corresponds to an established test site where controlled blasting was used to evaluate the magnitude of settlement resulting from dissipation of excess pore pressures in an unimproved and densified liquefiable soil, as reported by Gianella and Stuedlein (2017) and Mahvelati et al. (2020). The settlement measurements performed following dissipation of excess pore pressures are used in the remainder of this study to determine whether the random field model parameters describing their spatial distribution are consistent with those describing the characteristics of the soil deposit.

Post-Liquefaction Settlements Resulting from a Controlled Blasting Experiment and their Spatial Variability

The controlled blasting experiments conducted at the Hollywood, SC test site (Case A-1) consisted of detonating a sufficiently large series of explosives to induce and sustain liquefaction in an unimproved control zone for comparison to the response to a similar blast event applied to the displacement pile-improved Zones 1 through 4. The purpose of these experiments was to demonstrate the effectiveness of the densification programs to reduce the excess pore pressure ratios, r_u, defined as the ratio of dynamically-induced excess pore pressure and the existing vertical effective stress, relative to the unimproved zone and to quantify the reduction in post-blasting settlements possible due to the improvements. These experiments and corresponding results have been described extensively by Gianella and Stuedlein (2017) and Mahvelati et al. (2020), and the reader is referred to these works for further details. Blast event #4 at the unimproved zone produced sustained residual r_u of 100% to produce a bowl-shaped post-liquefaction settlement pattern characterized with a maximum settlement of 200 mm. The charge weights and pattern applied to the unimproved zone was therefore selected for application to Zones 1 – 4 (Table 1), and resulted in r_u ranging from 65 to 90% and average settlements, s, equal to 48 mm with s ranging from approximately 15 to 95 mm or about 1/6 to 1/3 of that of the unimproved zone (Gianella and Stuedlein 2017). Figure 7 presents the spatial variation of ground surface settlement measured following dissipation of excess pore pressures, which did not correspond directly to the magnitude of area replacement ratios or cone tip resistances associated with various levels of densification achieved in each zone. This observation formed the basis for the following inquiry.

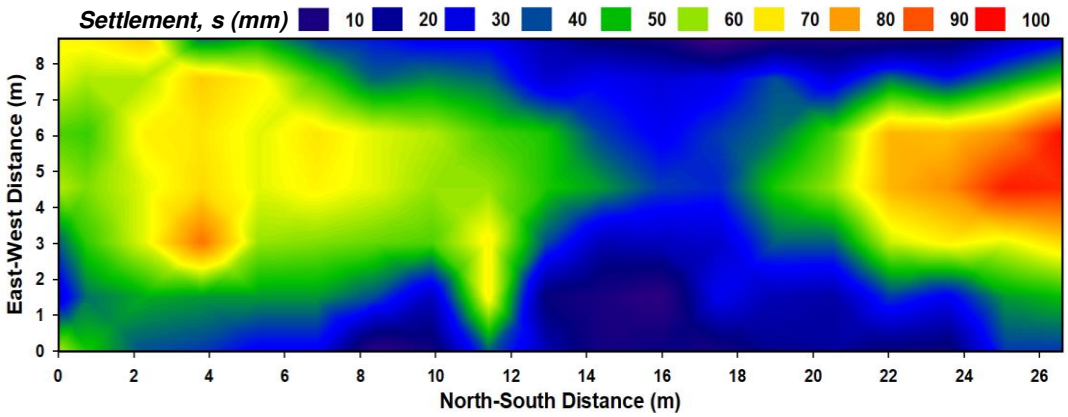


Figure 7. Spatially-distributed post-liquefaction settlements measured at Hollywood, SC and interpolated using ordinary kriging (Case A-1; data from Gianella and Stuedlein 2017).

Owing to its simple execution and assumptions, the expeditive method (Vanmarcke 1977) was used to estimate the horizontal scale of fluctuation, δ_h, and coefficient of inherent variability, $COV_{w,h}(s)$, corresponding to the blast-induced liquefaction settlement. The expeditive method was proposed by Vanmarke (1977) based on the observation that when approximating sample autocorrelation functions using the SQX ACF model, δcould be approximated as 80% of the average distance between the crossings of a measurement (e.g., q_t, s) through its fitted trend. Zhu et al. (2019) noted that this approximation is appropriate for normal random fields that are specified using the SQX model. The δ_h and $COV_{w,h}(s)$ were therefore estimated by fitting linear trends through the 19 settlement observations for each roughly north-south section on seven profiles extending from the east to the west of the site. Figure 8 presents selected representative profiles of post-liquefaction settlement in the

north-south direction and corresponding fitted trends. Table 3 summarizes the fitted linear trend functions, $COV_{w,h}(s)$, and δ_h derived from the implemented RFT framework.

In general, settlements decreased towards the south, as indicated by the negative trend slope (Table 3, Fig. 8). Two of the north-south settlement profiles, corresponding to east-west offsets of 3.04 and 4.56 m (Table 3), produced just two or three crossings of the trend in settlement; the expeditive method can overestimate δ_h if some crossing points are not sampled in the explorations (Ching et al. 2018), and common practice is to reject δ_h for trends exhibiting less trend crossings than desirable (e.g., Stuedlein et al. 2012; Bong and Stuedlein 2017; 2018). Such practice is consistent with recent findings by Zhu et al. (2019), in which the expeditive method may not be reliable when there are less than two observations within a distance δ_h; this is in agreement with Ching et al. (2018) and essentially conforming to the well-known signal processing theory attributed to Nyquist. Thus, the RFM parameters describing settlement for east-west offset sections at 3.04 and 4.56 m are not reported in Table 3. Considering the remaining settlement profiles, the average and range in $COV_{w,h}(s)$ were approximately 33% and 22.6 to 42.8%, respectively. Implementation of the expeditive method revealed δ_h that ranged from 3.81 to 5.63 m, with an average equal to 4.76 m.

Table 3. Summary of horizontal random field model parameters for blast-induced post-liquefaction settlements.

East-West Distance (m)	Mean s (mm)	Trend Function		$COV_{w,h}$ (%)	δ_h (m)	Comment
		Slope (mm/m)	Intercept (mm)			
0.00	31	-0.83	42	42.8	5.11	-
1.52	38	-0.33	43	39.1	4.18	-
3.04	55	-0.11	57	-	-	Insufficient # of trend crossings
4.56	65	0.58	58	-	-	Insufficient # of trend crossings
6.08	63	0.43	57	24.7	5.63	-
7.60	49	-1.02	62	22.6	3.81	-
8.72	34	-1.99	60	36.7	5.08	-
Mean	48	-0.47	54	33.2	4.76	
COV (%)	29.1	-191.8	15.4	27.1	15.6	

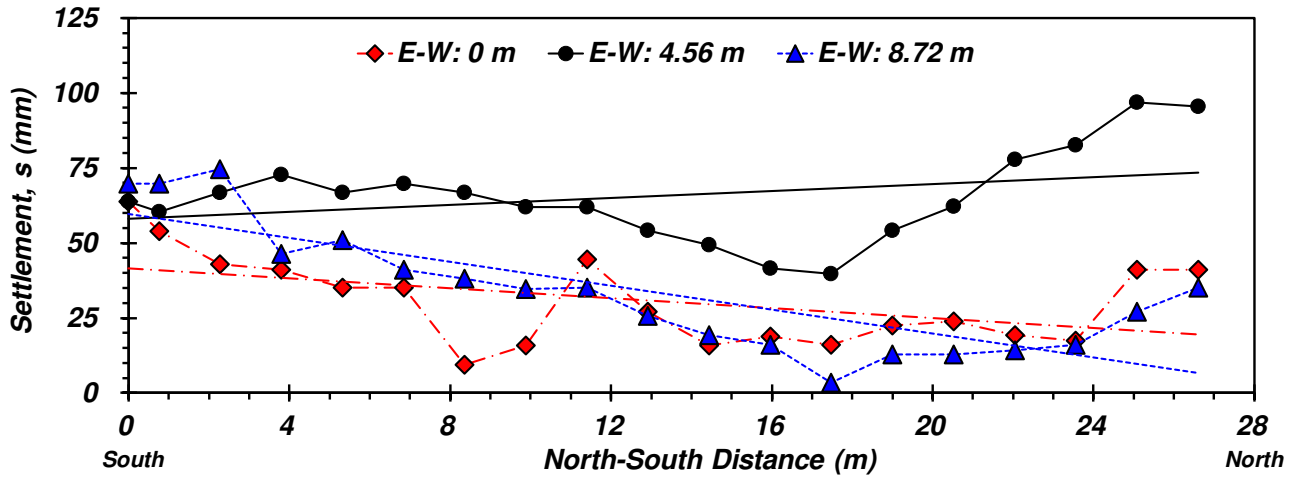


Figure 8. Representative horizontal profiles and fitted trends in the measured post-liquefaction settlement.

Possible Indicators of Settlement Potential: Horizontal RFM Parameters of Key Soil Properties

The potential for post-liquefaction settlement is dictated by several governing factors: the intensity of seismic loading, the cyclic resistance (or FS_L), and the relative density of the soil (Ishihara and Yoshimine 1992). These factors contribute to the maximum dynamic shear strain amplitude during loading, which ultimately controls the magnitude of post-seismic volume change (Ishihara and Yoshimine 1992; Yoshimine et al. 2006). The symmetric distribution of charges implemented by

Gianella and Stuedlein (2017) and used in Case A-1 served to limit variability in the resulting dynamic shear strains, however some variability in dynamic strains must be expected given the three-dimensional nature of blast-induced body waves (Jana and Stuedlein 2021). The investigation into the possible correlation of the spatially-varying post-shaking settlement measured at the ground surface (Fig. 7) to spatially-varying measures of soil resistance or constitutive response considered RFM parameters for q_t, the soil behavior type index, I_c (Robertson 2009), and fines content (FC), but could not explicitly account for the potential variability in dynamic shear strains.

Whereas q_t is implemented directly (following conditioning for overburden stress and other corrections), the use of I_c is intended to capture expected soil behaviors as a function of relative rates of drainage during dynamic loading, and FC relates to the compressibility of silty fines within the silty sand lenses present at the site. The calibrated geostatistical model of q_t and CPT sleeve friction, f_s, for the pre-densification subsurface conditions at the Hollywood, SC test site reported by Bong and Stuedlein (2017; 2018), and based on the initial 25 CPTs, was used to extract average pre-densification RFM parameters for q_t, I_c, and FC corresponding to the location of the settlement monitoring locations over the depths ranging from 2.5 to 11 m for the comparison. The site-specific CPT-based I_c-FC correlation proposed by Stuedlein et al. (2016), based on over 140 pairs of FC derived from split-spoon samples and co-located CPT soundings (within 0.76 m of borings), formed the basis for which to estimate the average RFM parameters for FC (Bong and Stuedlein 2017). Accordingly, the calibrated geostatistical model and the site-specific I_c-FC correlation allowed for the determination of the RFM parameters for each simulated sounding depth (i.e., 2 cm intervals) for estimating the average horizontal RFM parameters for q_t, I_c, and FC, and comparison to the horizontal RFM parameters of settlement derived for the north-south profiles presented above.

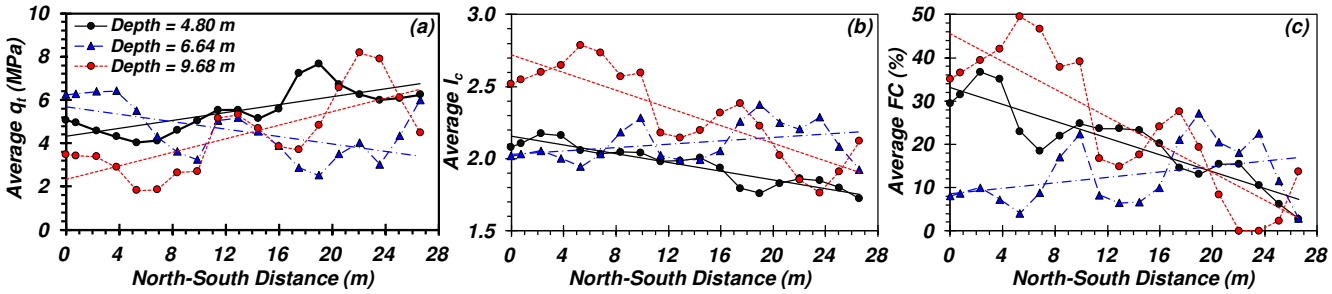


Figure 9. Representative horizontal profiles and fitted trends of (a) q_t, (b) I_c, and (c) FC averaged over the depths of 2.5 to 11 m for the E-W section offset of 4.56 m.

Representative average q_t, I_c, and FC profiles in the north-south direction for the 4.56 m east-west offset are shown in Figs. 9a – 9c. In general, the average q_t, I_c, and FC profiles exhibit a wide range in fluctuation across the north-south domain, regardless of the depth selected. Stuedlein and Bong (2017) noted that the variability within a given stratum may be as important as the variability in the stratum thickness in a given azimuthal bearing; in the case of the Hollywood, SC test site, the inherent variability of the stratum is of great importance due to the uniform thickness of the various strata that extended over the entire site. Figure 9 confirms that the inherent variability of the liquefiable layer is significant and should be expected to exhibit a wide range in post-shaking responses, as observed in Fig. 7.

The average horizontal RFM parameters, δ_h and $COV_{w,h}$, computed from each 2 cm incremental depth in the liquefiable layer, was computed for the three investigatory variables presented in Fig. 9 and are presented in Table 4. Similar to the determination of δ_h and $COV_{w,h}(s)$, parameter profiles for q_t, I_c, and FC with less than four trend crossings were neglected in the evaluation of δ_h and $COV_{w,h}$ for these variables. Interestingly, the breadth in average δ_h for q_t, I_c, and FC is rather narrow, ranging from 4.43 to 4.50 m, with a coefficient of variation of approximately 9%. On the other hand, the average and coefficient of variation of $COV_{w,h}$ varied greatly among these three variables, ranging from 3.9 to 44.5% and 38.0 to 42.1%. This indicates that variability in the fluctuating component of these variables is significant from depth to depth, and that looser and denser pockets of the sand and silty sand comprising the liquefiable layer may be expected to contribute to a spatially-variable liquefaction response as hypothesized by Bong and Stuedlein (2018).

Comparison of the Spatial Variability in Post-Liquefaction Settlements to Spatially-Variable Soil Characteristics

As noted above, the main objective of this comparison seeks to address whether the spatial variability in the consequences of liquefaction can be predicted using the random field model parameters representing the subsurface. Figure 10 presents a

comparison of δ_h and $COV_{w,h}$ of s, q_t, I_c, and FC. Considering the mean horizontal scale of fluctuation, the δ_h in settlement appeared best approximated by the soil behavior type index, I_c, with a percent difference of 5.6%. The percent difference between the δ_h in settlement and q_t and FC was 6.9 and 6.3%, respectively, indicating that these explanatory soil properties also appear to satisfactorily represent the observed spatial autocorrelation in settlement. Thus, it appears that the autocorrelation length of liquefaction-induced deformations may be correlated to pre-earthquake measurements.

Table 4. Summary of horizontal random field model parameters for q_t, I_c, and FC.

East-West Distance (m)	**Corrected Cone Tip Resistance, q_t**		**Soil Behavior Type Index, I_c**		**Fines Content, FC (%)**	
	$COV_{w,h}$ (%)	δ_h (m)	$COV_{w,h}$ (%)	δ_h (m)	$COV_{w,h}$ (%)	δ_h (m)
0.00	7.3	5.04	1.9	4.94	22.8	4.95
1.52	11.7	4.67	3.3	4.60	35.6	4.56
3.04	19.0	4.27	5.4	4.14	55.9	4.09
4.56	18.5	3.92	5.5	4.03	56.6	3.99
6.08	19.1	4.02	5.5	4.26	74.3	4.07
7.60	12.6	4.43	3.4	4.66	41.9	4.65
8.72	7.7	4.67	2.2	4.85	24.6	4.92
Mean	13.7	4.43	3.9	4.50	44.5	4.46
COV(%)	38.0	8.9	40.6	7.9	42.1	9.2

However, the comparison of the horizontal coefficient of inherent variability for the pre-event soil properties is shown to be quite different from that of the observed settlements (Fig. 10). Specifically, the $COV_{w,h}$ for q_t and I_c were quite different from that of s. While it is not surprising that there should be a strong difference between the pre-improvement q_t and the settlements measured following the blasting of the densified ground owing to the increase in cone tip resistance demonstrated in Fig. 6, the soil composition estimated from the soil behavior type I_c should not be expected to change following densification as the driving of displacement piles does not alter the constituents of the improved soils in the way that improvements such as deep soil mixing does. In general, the $COV_{w,h}$ of FC exhibited the greatest similarity to that of the observed settlement, with an absolute difference of 11% and percent difference of 34%. The overall predictive strength of the RFM parameters for FC is intuitive since the compressibility of silty sand increases with silty fines content (Bandini and Sathiskumar 2009), and the amount of silty fines at a given location within the subsurface is relatively unchanged by this densification-based ground improvement. Nonetheless, a multivariate relationship should exist between the coefficient of inherent variability of relevant soil properties and the manifestation of post-liquefaction settlement at a particular site, and the reliance on a single parameter is not advised.

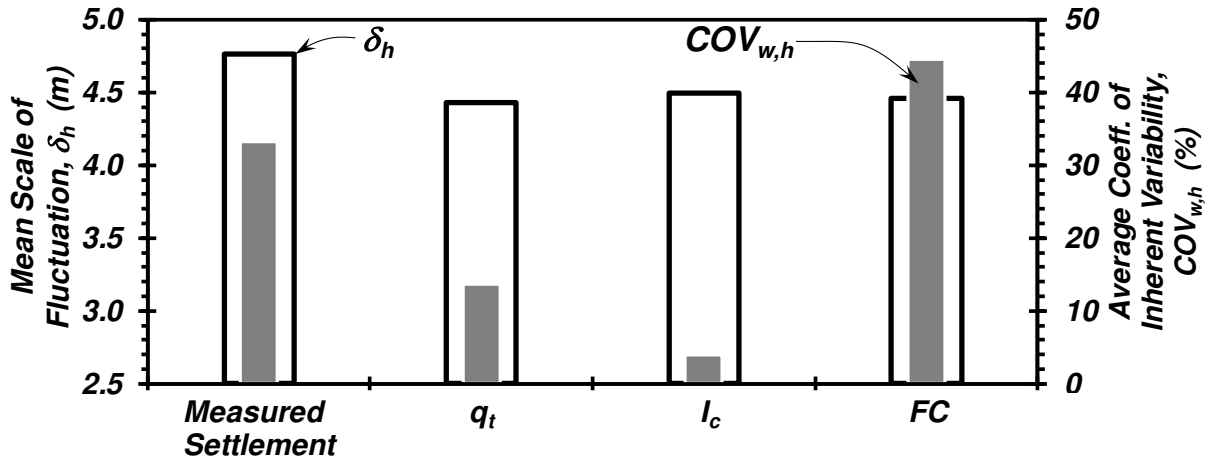


Figure 10. Comparison of RFM parameters for observed post-liquefaction settlements and in-situ, pre-improvement soil properties.

The above discussion pertained to analyses that leveraged previously-developed geostatistical models to investigate whether the characteristics describing the spatial variability of post-liquefaction settlements could be linked to those associated with the pre-improved test site. Another limitation of the previous comparison is that just one measure of soil resistance was used

in the comparison, namely the pre-improvement q_t. To address these limitations, the correspondence of soil properties measured following improvement to the magnitude of settlement was investigated using an expanded set of variables measured or deduced at 12 locations where post-improvement CPTs were conducted. Since the I_c and FC computed and correlated from site-specific CPT data, respectively, were significantly affected by the changes in lateral stress following densification (Nguyen et al. 2014), the comparison relies upon the pre-improvement I_c and FC.

Figure 11 presents the correlation between the average post-improvement q_t, q_{c1N}, q_{c1Ncs}, and D_r over the range in depths of 2.5 to 11 m, where q_{c1N} and q_{c1Ncs} correspond to the liquefaction-triggering procedures proposed by Boulanger and Idriss (2015) and D_r was computed using the CPT-based correlation by Mayne (2007). These four post-improvement variables exhibited similarly poor correlation to the post-liquefaction settlement of the ground surface at the location of the 12 CPTs. Generally, the greater the average q_t, the smaller the resulting post-liquefaction settlement is expected to be owing to the increased cyclic resistance and lower excess pore pressure generated during a dynamic event. Instead, Zone 3 exhibited smaller settlements despite the overall lower q_t due to the role of other factors that may govern the performance of the improved ground, including the area replacement ratio, pile toe condition, and the fines content of the soil in the immediate vicinity of the improvements. The correlation between settlement and pre-densification I_c is moderately strong; I_c facilitates differentiation between "sand-like" and "clay-like" behavior and thus addresses liquefaction susceptibility (and its consequences) to a degree; however, there is difficulty identifying the soil behavior type of transitional soils (e.g., silty sands, sandy silts, clayey silts, and clayey sands), and its magnitude does not readily distinguish the nature of the soil response to undrained shear (e.g., degree of contraction vs. dilation).

Figure 11 shows that the pre-improvement FC exhibited the highest correlation (0.76) with the settlement measured, indicating that the greater the average FC within the improved liquefiable layer, the greater the settlement measured. This is consistent with the observation that the RFM parameters describing the spatial variability of the post-liquefaction settlement are similar to those of FC in the liquefiable layer, and consistent with the increased compressibility of silty sands with increases in fines content noted earlier. Note that the FC correction to liquefaction resistance commonly adopted in triggering analyses addresses the role of partial drainage in silt-rich soils during penetration, which serves to reduce the penetration resistance relative to clean sands (Krage et al. 2014). The correction is necessary to provide the basis for a clean sand base liquefaction triggering curve (Youd et al. 2001), but the actual role of silty fines on liquefaction triggering is unclear when considering the various studies on reconstituted specimens (e.g., Hazirbaba and Rathje 2009). However, the increased compressibility of silty sands relative to clean sands is well understood; therefore, based on the preceding analysis, the use of the spatial variability in FC appears to represent a promising indicator for the prediction of the spatial variability in the consequences of liquefaction.

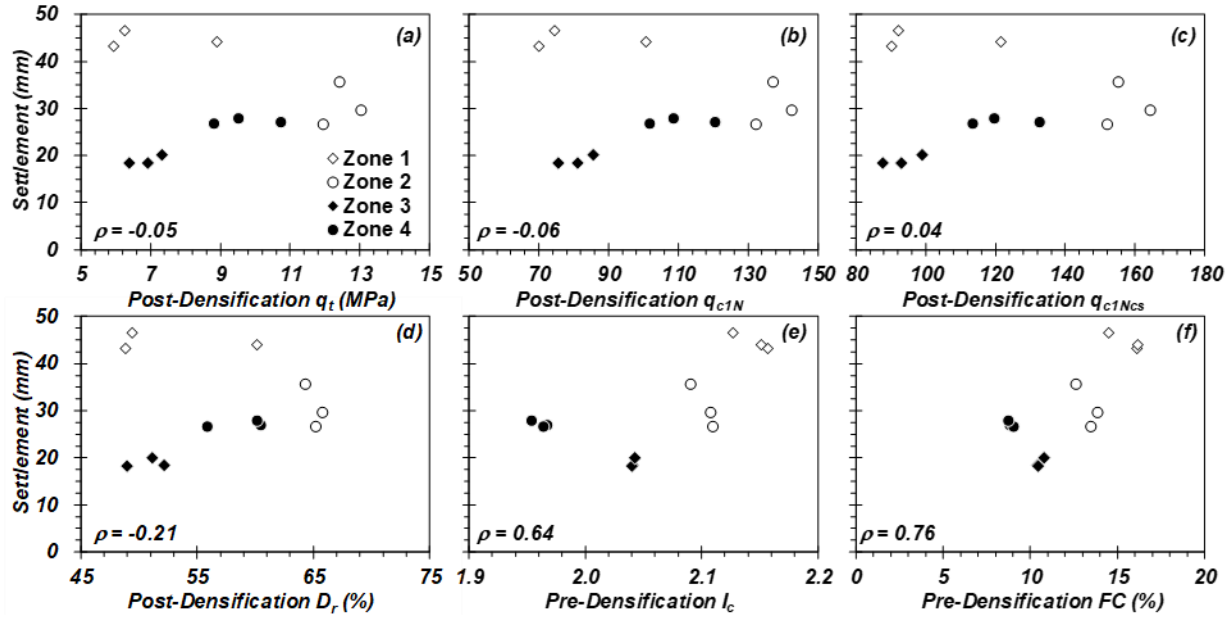


Figure 11. Relationships between various pre- and post-densification soil properties and post-liquefaction settlement, indicating the apparent correlations between pre-densification measures and post-event deformations.

CONCLUSION

This case history-based study conducted in two parts sought to address: (1) the changes in vertical spatial variability of liquefiable soils following densification with various ground improvement techniques, and (2) whether the observed random field characteristics of the spatial distribution in post-liquefaction settlements may be estimated using the random field model parameters describing the spatial variability of relevant soil parameters. The authors have attempted to leverage case history data to demonstrate that random field theory does indeed have a role in the geotechnical engineering profession and that useful outcomes are readily obtained, given sufficient subsurface information which can be leveraged for the purpose. Based on the investigations carried out herein, the following conclusions regarding the change in vertical spatial variability following densification may be drawn:

1. The increase in mean q_t varied with the area replacement ratio implemented and the initial relative density of the liquefiable soils;

2. On average, the vertical coefficient of inherent variability in q_t decreased following improvement, indicating that the densified soil became more homogenous as a result of the ground improvement;

3. In general, the vertical scale of fluctuation representing the autocorrelation length of q_t increased as a result of densification, providing additional support for the increase in soil homogeneity following improvement; and,

4. There appears to be a dependence on the change in the scale of fluctuation following densification to the pre-improvement autocorrelation length.

One of the case histories evaluated in the first portion of the paper was then used to establish whether the spatial variability in the consequences of liquefaction (i.e., settlement) could be predicted using the spatial variability of certain soil properties. This objective was informed by observations that the spatial variability of soils often contributes to variability in the response of soils and supported structures during post-earthquake reconnaissance. The random field characteristics of relevant soil parameters, including the pre-densification cone tip resistance, soil behavior type index, and fines content, formed the basis for the comparison of the horizontal scale of fluctuation and coefficient of inherent variability of these properties to post-liquefaction settlements observed in variously densified ground.

This study clearly showed that the autocorrelation structure of the liquefiable soil as estimated using the horizontal scale of fluctuation in fact could predict the autocorrelation characteristics of the observed deformations. Whereas the coefficient of inherent variability of cone tip resistance and soil behavior type index could not adequately represent the variability in settlements, that of the fines content did indeed appear to approximate the random field representation of deformations. Although the inherent variability in the magnitude of post-liquefaction settlements arises from complex soil mechanical and dynamical interactions, a relatively strong correlation between soil behavior type index and fines content to the post-liquefaction settlements of the densified ground demonstrate that the random field theory implemented herein holds significant promise for estimating the variability in the consequences of liquefaction.

REFERENCES

Bandini, P., and Sathiskumar, S. (2009). "Effects of silt content and void ratio on the saturated hydraulic conductivity and compressibility of sand-silt mixtures." *J. Geotech. Geoenv. Eng.*, 135(12), 1976-1980.

Broms, B. (1966). Methods of calculating the ultimate capacity of piles – a summary. *Sols-Soils*, 5(18–19), 21-32.

Bong, T. and Stuedlein, A.W. (2017). "Spatial Variability of CPT Parameters and Silty Fines in Liquefiable Beach Sands." *J. Geotech. Geoenv. Eng.*, 143(12).

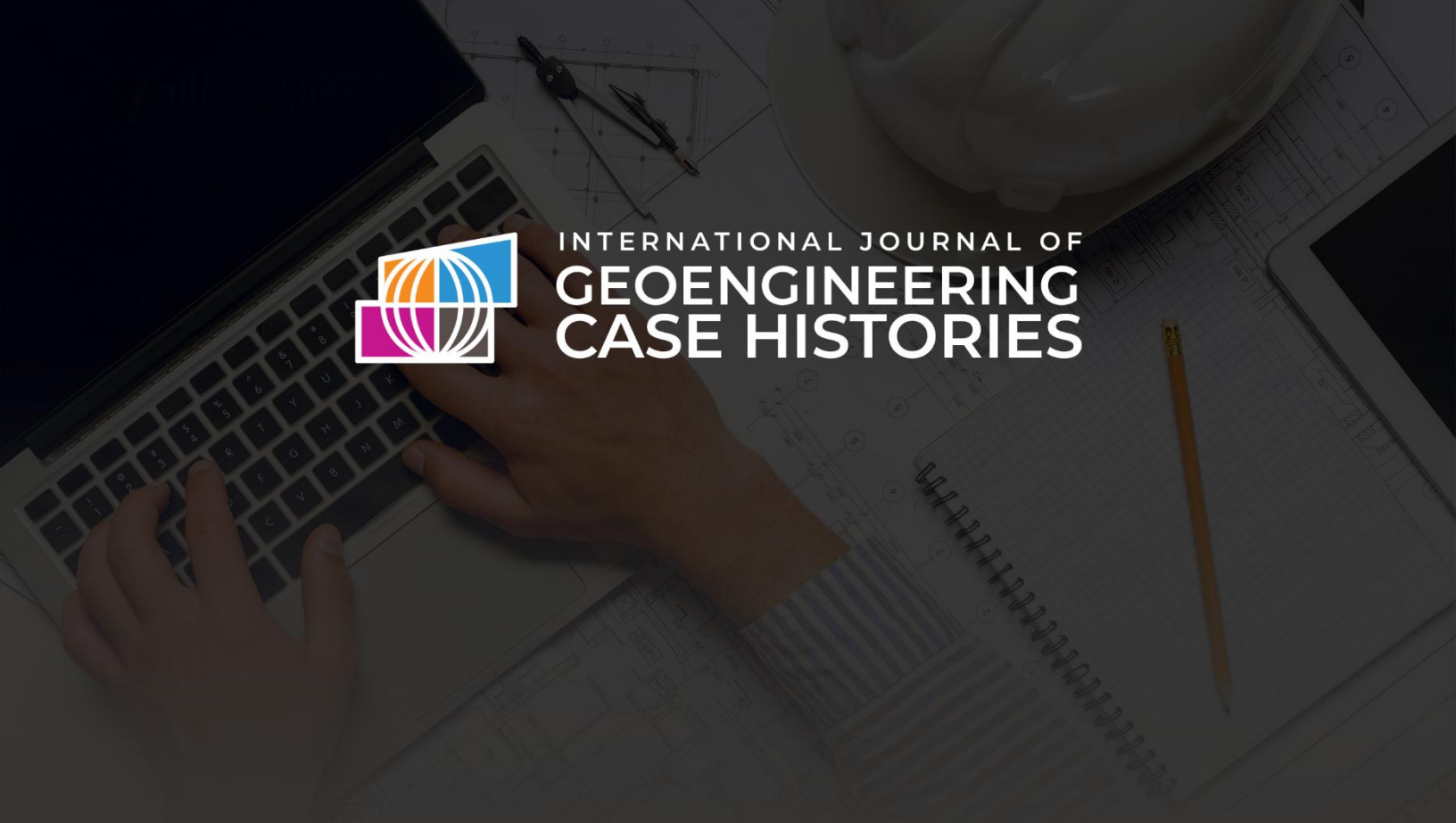
Bong, T. and Stuedlein, A.W. (2018). "Effect of Cone Penetration Conditioning on Random Field Model Parameters and Impact of Spatial Variability on Liquefaction-induced Differential Settlements." *J. Geotech. Geoenv. Eng.*, 144(5).

Boulanger, R. W., and Idriss, I. M. (2015). "CPT-based liquefaction triggering procedure." *J. Geotech. Geoenviron. Eng.*, 10.1061/(ASCE)GT .1943-5606.0001388, 04015065.

Cami, B., Javankhoshdel, S., Phoon, K. K. & Ching, J. Y. (2020). "Scale of Fluctuation for Spatially Varying Soils: Estimation Methods and Values." *ASCE-ASME Journal of Risk and Uncertainty in Engineering Systems*, Part A: Civil Engineering, 6(4).

Ching, J., Wu, T.-J., Stuedlein, A.W., Bong, T. (2018). Estimating horizontal scale of fluctuation with limited CPT soundings. *Geoscience Frontiers*, 9, 1597-1608.
Cubrinovski, M., et al. (2011). "Geotechnical aspects of the 22 February 2011 Christchurch earthquake." *Bull. N. Z. Soc. Earthquake Eng.*, 44(4), 205–226.
Fenton, G. A., and Vanmarcke, E. H. (1998). "Spatial variation in liquefaction risk." *Geotechnique*, 48(6), 819–831.
Gianella, T.N. and Stuedlein, A.W. 2017. Performance of Driven Displacement Pile-Improved Ground in Controlled Blasting Field Tests. *J. Geotech. Geoenv. Eng.*, 143(9).
Griffiths, D. V., and Fenton, G. A. (2001). "Bearing capacity of spatially random soil: The undrained clay Prandtl problem revisited." *Geotechnique*, 54(4), 351–359.
Hazirbaba, K. and Rathje, E.M. (2009). "Pore Pressure Generation of Silty Sands due to Induced Cyclic Shear Strains," *J. Geotech. Geoenv. Eng.*, 135(12), 1892–1905.
Ishihara, K., and Yoshimine, M. (1992). Evaluation of settlements in sand deposits following liquefaction during earthquakes." *Soils and Foundations*, 32(1), 173–188.
Jaksa, M.B. (1995). *The Influence of Spatial Variability on the Geotechnical Design Properties of a Stiff, Overconsolidated Clay,* Ph.D. Thesis, Faculty of Engineering, University of Adelaide.
Jaksa, M.B. Jaksa, M. B., Brooker, P. I., and Kaggwa, W. S. (1997). "Inaccuracies associated with estimation of random measurement errors." *J. Geotech. Geoenviron. Eng.,* 123(5), 393–401.
Jana, A. and Stuedlein, A.W. (2021). "Dynamic, In-situ, Nonlinear-Inelastic Response of a Deep, Medium Dense Sand Deposit." *J. Geotech. Geoenv. Eng.*, 147(6).
Krage, C.P., DeJong, J. T., & Wilson, D. W. (2014). "Variable penetration rate cone testing in sands with fines." *Geo-Congress 2014*: *Geo-characterization and Modeling for Sustainability*, GSP No. 234, ASCE, Reston, VA., 170-179.
Mahvelati, S., Coe, J.T., Stuedlein, A.W., Asabere, P., Gianella, T.N., Kordjazi, A. (2020). "Recovery of Small-Strain Stiffness Following Blast-Induced Liquefaction Based on Shear Wave Velocity Measurements." *Can. Geot. J.*
Massarsch, K. R., Wersäll, C., & Fellenius, B. H. (2020). "Horizontal stress increase induced by deep vibratory compaction." *Proceedings of the Institution of Civil Engineers-Geotechnical Engineering*, 173(3), 228-253.
Mayne, P. W. (2007). NCHRP Synthesis 368: Cone penetration testing. *Transportation Research Board*, Washington, DC.
Mayne, P.W. and Kulhawy, F.H (1982). "K_0-OCR Relationships in Soil." *J. Geotech. Eng. Div.*, 108(6), 851-872.
Montgomery, J., and Boulanger, R. W. (2017). "Effects of spatial variability on liquefaction-induced settlement and lateral spreading." *J. Geotech. Geoenv. Eng.*, 143(1).
Meyerhof, G. G. (1959). "Compaction of sands and bearing capacity of piles," *J. Soil Mechanics Foundations Div.*, 85(SM6), 1-30.
Nguyen, T.V., Shao, L., Gingery, J., and Robertson, P.K. (2014). "Proposed modifications to CPT-based liquefaction method for post-vibratory ground improvement." *GeoCongress 2014*, GSP No. 234, ASCE, 1120-1132.
Plantema, I. G., and Nolet, C. A. (1957). "Influence of pile driving on the sounding resistance in a deep sand layer." *Proc., 4th Int. Conf. Soil Mechanics and Found Engineering*, Balkema, Rotterdam, Netherlands, 52–55.
Robertson, P. K. (2009). "Interpretation of cone penetration tests – a unified approach." *Can. Geot. J.*, 46(11), 1337-1355.
Robinsky, E.I. and Morrison, C.F. (1964) "Sand Displacement and Compaction around Model Friction Piles," *Can. Geo. J.*, 1(2), 81 – 93.
Rollins, K. M., Price, B. E., Dibb, E., and Higbee, J. B. (2006). "Liquefaction mitigation of silty sands in Utah using stone columns with wick drains." *Ground modification and seismic mitigation*, ASCE, Reston, VA.
Rollins, K., Wright, A., Sjoblom, D., White, N., and Lange, C. (2012). *CPT evaluation of liquefaction mitigation with stone columns in interbedded soils*, UDOT Report No. UT-12.15, Brigham Young Univ.
Slocombe, B.C., Bell, A.L., and Baez, J.I. (2000). "The densification of granular soils using vibro methods." *Geotechnique*, 50(6), 715-725.
Stuedlein, A.W. (2010). "Shear Wave Velocity Correlation for Puyallup River Alluvium." *J. Geotech. Geoenv. Eng.*, 136(9), 1298-1304.
Stuedlein, A.W., Abdollahi, A., Mason, H.B., and French, R. (2015). "Shear Wave Velocity Measurements of Stone Column Improved Ground and Effect on Site Response," *International Foundation Congress and Equipment Expo*, Geotechnical Special Publication No. 256, San Antonio, Reston, VA., 2306-2317.
Stuedlein, A. W. and Bong, T. (2017). "Effect of spatial variability on static and liquefaction-induced differential settlements." *Geo-Risk 2017: Keynote Lectures,* GSP No. 282, 31-51.
Stuedlein, A.W., and Allen, M.L. (2018). "A Case History of Liquefaction Mitigation using Driven Displacement Piles." *IFCEE 2018: Recent Dev. Geotech. Eng. Prac.*, 253-262.
Stuedlein, A.W., Kramer, S.L., Arduino, P., and Holtz, R.D. (2012). "Geotechnical Characterization and Random Field Modeling of Desiccated Clay". *J. Geotech. Geoenv. Eng.*, 138(11), 1301-1313.

Stuedlein, A.W. and Gianella, T.N. (2016). “Observations on the Effect of Driving Sequence and Spacing on Displacement Pile Capacity.” *J. Geotech. Geoenv. Eng.*, 143(3).
Stuedlein, A.W., Gianella, T. N., and Canivan, G. (2016). “Densification of Granular Soils Using Conventional and Drained Timber Displacement Piles.” *J. Geotech. Geoenv. Eng.*, 142(12).
Sy, A. (2018). “Challenges in Geoseismic Upgrade of Bridges in the Fraser Delta, BC, Canada.” *Geot. Earthq. Eng. Soil Dyn. V: Liquefaction Triggering, Consequences, and Mitigation*, ASCE, Reston, VA., 148-159.
Uzielli, M., Vannucchi, G., and Phoon, K.K. (2005). “Random field characterisation of stress-normalised cone penetration testing parameters.” *Geotechnique*, 55(1), 3-20.
Vanmarcke, E.H. (1977). “Probabilistic Modeling of Soil Profiles.” *J. Geotech. Geoenv. Eng.*, 103(GT11), 1227-1246.
Vanmarcke, E.H., (1983). *Random Fields: Analysis and Synthesis*, MIT Press, Cambridge, MA, USA.
Yoshimine, M., Nishizaki, H., Amano, K., and Hosono, Y. (2006). “Flow deformation of liquefied sand under constant shear load and its application to analysis of flow slide of infinite slope.” *Soil Dyn. Earth. Engrg*., 26, 253-264.
Youd, T.L. (1972). “Compaction of sands by repeated shear straining.” *J. Soil Mech. Found. Div.*, 98(7), 709-725.
Youd, T.L., et al. (2001). “Liquefaction resistance of soils: summary report from the 1996 NCEER and 1998 NCEER/NSF workshops on evaluation of liquefaction resistance of soils.” *J. Geotech. Geoenv. Eng.*, 127(4), 297-313.
Zhu, Y.-X., Zheng, S., Cao, Z.-J., and Li, D.-Q. (2019). “Revisiting the Relationship between Scale of Fluctuation and Mean Cross Distance.” *Proc., 13th Int. Conf. App. Stat. Prob. Civil Engrg. (ICASP13)*, Seoul, South Korea.



INTERNATIONAL JOURNAL OF
GEOENGINEERING
CASE HISTORIES

The Journal's Open Access Mission is generously supported by the following Organizations:

dar
a Sidara company

Geosyntec consultants
engineers | scientists | innovators

ConeTec

MUD BAY DRILLING
LANKELMA
Geotech DRILLING

ENGEO
Expect Excellence

Access the content of the ĪSSMGE Īnternational Journal of Geoengineering Case Histories at:
www.geocasehistoriesjournal.org

Downloaded: Thursday, November 19 2026, 08:41:33 UTC